HHS Public Access

Author manuscript

Nat Immunol. Author manuscript; available in PMC 2017 March 26.

Published in final edited form as:

Nat Immunol. 2016 November ; 17(11): 1312–1321. doi:10.1038/ni.3559.

The ubiquitin ligase HUWE1 regulates hematopoietic stem cell maintenance and lymphoid commitment

Bryan King[1,2,3,8], **Francesco Boccalatte**[1,2,8], **Kelly Moran-Crusio**[1,2,4], **Elmar Wolf**[5], **Jingjing Wang**[1,2], **Clarisse Kayembe**[1,2], **Charalampos Lazaris**[1,2,7], **Xiaofeng Yu**[1,2], **Beatriz Aranda-Orgilles**[1,2], **Anna Lasorella**[6], and **Iannis Aifantis**[1,2]

[1]Department of Pathology, NYU School of Medicine, New York, NY 10016, USA

[2]Laura and Isaac Perlmutter Cancer Center, New York, NY 10016, USA

[3]Cancer Biology and Genetics Program, Memorial Sloan Kettering Cancer Center, New York, NY 10065, USA

[4]Department of Medicine, Quinnipiac University Netter School of Medicine, NH-MED, Hamden, CT 06518, USA

[5]Comprehensive Cancer Center Mainfranken and Department of Biochemistry and Molecular Biology, Biocenter, University of Würzburg, Am Hubland, 97074 Würzburg, Germany

[6]Department of Pathology and Cell Biology and Pediatrics, Institute for Cancer Genetics, Columbia University Medical Center, New York, NY 10019, USA

[7]Center for Health Informatics and Bioinformatics, NYU School of Medicine, New York, NY, 10016, USA

Abstract

Hematopoietic stem cells (HSCs) are dormant in the bone marrow and can be activated in response to diverse stresses to replenish all blood cell types. Here we identify the ubiquitin ligase Huwe1 as a crucial regulator of HSC functions via its post-translational control of N-myc. We found *Huwe1* to be essential for HSC self-renewal, quiescence and lymphoid fate specification. Using a novel fluorescent fusion allele (*Mycn*^{M}), we observed that N-myc expression was restricted to the most immature, multipotent stem and progenitor populations. N-myc was upregulated in response to

Correspondence should be addressed to I.A. (iannis.aifantis@nyumc.org). or B.K. (kingb2@mskcc.org).

[8]These authors have contributed equally

ACCESSION CODES

RNA-sequencing, ChIP-sequencing and microarray data were deposited into the Gene Expression Omnibus (GEO) with the following accession codes: GSE85488

AUTHOR CONTRIBUTIONS

B.K. and I.A. designed the study and prepared the manuscript. B.K. performed most of the experiments described in the manuscript. F.B. completed experiments and focused on N-myc genomic and transcriptomic studies. K.M-C. initiated the *Huwe1* cKO *in vivo* analysis. E.W. performed the N-myc ChIP-Seq. F.B. and B.A-O. analyzed the MYCN ChIP-Seq data. J.W. and C.K. were responsible for animal husbandry. C.L. provided bioinformatics analysis and guidance. X.Y. designed the *Mycn* mCherry targeting vector. A.L. provided *Huwe1*–floxed mice and helped with data analysis.

COMPETING FINANCIAL INTERESTS

The authors declare no competing financial interests.

stress or upon loss of Huwe1, leading to increased proliferation and stem cell exhaustion. *Mycn* depletion reversed most of these phenotypes *in vivo*, suggesting that the attenuation of N-myc by Huwe1 is essential to reestablish homeostasis following stress.

Introduction

HSCs have the unique capacity to self-renew and differentiate into all mature blood lineages. Although HSCs are a predominantly quiescent population, they can respond dynamically to extrinsic cues, such as injury and infection[1]. HSC exhaustion is the phenomenon whereby this typically quiescent population is driven to proliferate abnormally and the balance between asymmetric, self-renewing divisions is skewed toward rapid symmetric divisions, eventually leading to a premature depletion of the stem cell pool[2]. Chronic inflammation, inhibition of cyclin-dependent kinase inhibitors (CKI) or loss of particular angiocrine factors in the bone marrow niche can all lead to stem cell exhaustion[3]. Thus, to prevent stem cell exhaustion, mechanisms must exist in HSCs to attenuate proliferative signals.

The transition from the resting (G_0) to activated (G1) cell state is primarily driven by the accumulation of biomass, manifested by increased transcriptional and translational activity along with greater uptake and anabolism of biosynthetic precursors[4]. The Myc family of proto-oncogenes (c-Myc, N-myc and L-myc) are particularly relevant in this context, as these have been shown to influence transcription of a wide range of genes that are required for cell growth and DNA replication[5, 6]. *Myc* and *Mycn* mRNAs are expressed at roughly equivalent levels in HSCs[7]. Conditional deletion of *Myc* has been shown to inhibit differentiation of HSCs whereas deletion of both *Myc* and *Mycn* genes leads to rapid depletion of the stem cell pool[7, 8]. As proteins, c-Myc and N-myc exhibit extensive post-translational modifications and are remarkably unstable[9–11]. Turnover of Myc proteins is determined by a cascade of phosphorylation and ubiquitylation events, which target them for ubiquitin-mediated proteolysis[12, 13].

We and others have previously demonstrated the critical role of the SCF^{Fbxw7} ubiquitin ligase as a regulator of HSC quiescence[14–16] and shown that stem cell exhaustion observed in *Fbxw7* conditional knockout mice is dependent on abundance of c-Myc protein[14]. The HECT family ubiquitin ligase Huwe1 (also referenced as Mule or ARF-BP1) has been shown to ubiquitylate many of the same substrates as Fbxw7, including Mcl1, c-Myc and N-myc[17–19]. Furthermore, *Huwe1* has been previously implicated as a determinant of neural stem cell self-renewal and differentiation[20]. Therefore, we hypothesized that the two ligases might act in a similar or concerted fashion in HSCs.

Here we report that conditional knockout of *Huwe1* in the hematopoietic system led to a loss of HSC self-renewal and impaired lymphoid specification at the earliest stages of differentiation. Using novel fluorescent fusion knock-in alleles, we observe at the single-cell level that loss of Huwe1 leads to stabilization of its substrate N-myc. Attenuation of N-myc by Huwe1 was essential to maintain quiescence of adult HSCs, as we demonstrate that depletion of *Mycn* in *Huwe1*-deficient HSC led to restoration of the stem cell pool. This work further illustrates the complex regulation of Myc transcription factors by the ubiquitin proteasome system in immune development.

Results

Huwe1 is essential for HSC maintenance and recovery from stress

Analysis of RNA sequencing data from sorted populations of hematopoietic cells revealed that HECT, UBA and WWE domain containing 1 (*Huwe1*) was among the most highly expressed genes related to ubiquitin conjugation in HSCs (Supplementary Fig. 1a)[21]. *Huwe1* expression decreased during early stages of differentiation, but was abundantly expressed in mature lymphoid populations (B, T and NK cells) (Supplementary Fig. 1b). To study whether Huwe1 has a role in hematopoiesis, *Huwe1* conditional knockout ("floxed") mice were crossed to the pI:pC-inducible Mx1-Cre transgenic line to induce deletion of *Huwe1* in HSCs (and their progeny) in adult mice. At early timepoints post-pI:pC administration (4–6 weeks), a slight, but significant, increase in phenotypic HSCs (Lineage-negative (Lin^-) $Kit^+Sca1^+CD150^+CD48^-$) was observed in *Huwe1*-deficient bone marrow (Supplementary Fig. 1c). However, at later time points of analysis (4–6 months post-deletion), HSCs were severely reduced, in both frequency and absolute number, in the bone marrow of $Huwe1^{F/Y}$Mx1-Cre^+ mice (Fig. 1a–c), suggesting that an expansion and subsequent contraction of the self-renewing HSC population had occurred following loss of *Huwe1*.

To test the consequences of *Huwe1* loss on HSC function *in vivo*, bone marrow from $Huwe1^{F/Y}$Mx1-Cre^+ or $Huwe1^{+/Y}$Mx1-Cre^+ donors was transplanted competitively with an equal number of wild-type bone marrow cells into lethally irradiated congenic recipients (Fig. 1d). pI:pC was administered to recipients 3 weeks post-transplant. Contribution from the *Huwe1*-deficient donors to peripheral blood chimerism declined significantly and was virtually undetectable 12 weeks after pI:pC treatment. These data suggested that the stem cell defect in *Huwe1*-deficient mice is cell-intrinsic and cannot be attributed to failure to home in bone marrow, as we observed these effects with deletion following engraftment. Similarly, the *in vitro* colony-forming ability of isolated *Huwe1*-deficient hematopoietic stem and progenitor cells (HSPCs: $Lin^-Kit^+Sca1^+$) was also impaired upon serial passaging (Supplementary Fig. 1d). Analysis of the bone marrow of transplant recipients revealed a significant reduction in total donor-derived cells and a profound loss of donor-derived HSCs in the *Huwe1*-deficient cohort (Supplementary Fig. 1e,f).

Since the onset of hematopoietic defects in *Huwe1* conditional knockout mice was more rapid upon transplantation, we further investigated how *Huwe1*-deficient HSCs would respond to acute stress. Treatment with the chemotherapeutic agent 5-fluorouracil (5-FU) specifically ablates rapidly dividing hematopoietic progenitor cells and subsequently induces cycling of otherwise quiescent HSC to replenish these progenitor pools[22]. Therefore, we tested how *Huwe1*-deficient mice would respond to serial 5-FU challenge. In this context, *Huwe1*-deficient mice exhibited markedly decreased survival when compared to wild-type mice (Fig. 1e). We hypothesized that this increased susceptibility to repetitive 5-FU challenge was due an inability of *Huwe1*-deficient HSCs to reenter quiescence. Accordingly, in wild-type bone marrow, ~70% of HSC were in resting phase (G_0) 14d after 5-FU treatment, whereas only half (36%) of *Huwe1*-deficient HSCs were in G_0 at the same time point (Supplementary Fig. 1g). We also found a significant decrease in quiescence in

Huwe1-deficient HSCs under steady state conditions (Fig. 1f), although to a lesser extent than following 5-FU.

To avoid any potential complications due to activation of interferon response in the Mx1-Cre model[23], we also generated *Huwe1* conditional knockouts using the *Vav1*-Cre transgene. *Vav1*-Cre is pan-hematopoietic and labels the vast majority of fetal HSCs in lineage-tracing experiments by E13.5[24]. Fetal livers from developing *Huwe1*-deficient or wild-type embryos (E18.5) exhibited no difference in HSC number (Supplementary Fig. 2a,b), but gave rise to significantly fewer colonies *in vitro* (Supplementary Fig. 2c). Conversely, adult *Huwe1*$^{F/Y}$ *Vav1*-Cre^{+} mice, had significantly fewer bone marrow HSCs compared to their wild-type littermates and the latency of this phenotype was notably shorter than in the inducible Mx1-Cre model (Fig. 2a). Taken together, these findings suggested that *Huwe1* is essential for quiescence and self-renewal of adult HSC both in steady-state and under conditions of stress.

Huwe1 is essential for early lymphoid specification

Interestingly, a profound reduction in early lymphoid progenitors and developing B cells was observed in the bone marrow of *Huwe1*-deficient mice (Fig. 2a–c). Erythroid and myeloid populations in these mice were not reduced (Fig. 2d), suggesting this reduction was not merely a consequence of declining HSC function. Early T cell commitment was also diminished in these mice, resulting in thymii that were significantly smaller in size and decreased in cellularity (Fig. 2e and Supplementary Fig. 3a). Thus, we concluded that *Huwe1* also has a crucial role in early fate decisions in HSCs, demonstrated by the loss of the earliest lymphoid-biased or restricted progenitors (Flt3^{+} MPPs and CLPs) in the bone marrow[25]. This effect was cell intrinsic, as sorted *Huwe1*-deficient HSPCs were also defective or delayed in their ability to give rise to B and T cells in OP9 stromal co-cultures (Supplementary Fig. 3b,c).

In contrast, approximately half of *Huwe1*$^{F/Y}$Vav1-Cre^{+} mice that were aged beyond four months exhibited signs of myelo-proliferation, accompanied by reduced hemoglobin and red blood cell counts (Supplementary Fig. 4a,b) and slightly elevated white blood cell (WBC) counts (Supplementary Fig. 4c). The majority of nucleated cells in the peripheral blood were granulocytes or monocytes (Supplementary Fig. 4d,e). The spleens of these aged mice also had a profoundly disrupted architecture characterized by loss of distinguishable boundary between white and red pulp and a 2-fold or greater expansion in CD11b^{+} cells (Supplementary Fig. 4f). These observations implied that Huwe1 loss alters differentiation balance leading to the significant loss of lymphoid progenitors and, in a subset of mice, indicators of myelo-proliferative neoplasms.

Mapping N-myc and c-Myc proteins *in vivo*

We hypothesized that the hematopoietic defects exhibited in *Huwe1*-deficient mice are a consequence of changes in the activity of Myc proteins. *Myc* and *Mycn* are the two Myc family genes that are predominantly expressed in hematopoietic progenitors[7]. Since the c-Myc–GFP fusion allele (*Myc*^{G}) has proven useful for determining post-transcriptional regulation of c-Myc in heterogeneous populations of cells[14, 26, 27], we sought to generate a

similar fusion allele for N-myc. A targeting construct was generated where mCherry cDNA was cloned in frame with the first translated ATG within the *Mycn* gene. (Supplementary Fig. 5a). N-myc immunoblot analysis of normal and targeted ES cells confirmed that an immunoreactive protein product of approximately 95 kDa was expressed exclusively in the properly targeted ESCs (Fig. 3a). Consequently, a significant shift in mCherry fluorescence was observed in ESCs that expressed the N-myc fusion product (Fig. 3b). Two independent ESC clones were used to establish *Mycn*–mCherry ($Mycn^{M}$) mouse lines where the fusion protein would be expressed in all tissues. Intercrossing of $Mycn^{M/+}$ mice resulted in homozygous $Mycn^{M/M}$ pups at the expected Mendelian ratio and these mice developed to adulthood without any discernable defects.

Although robust expression of N-myc–mCherry was observed in embryonic stem cells, mCherry fluorescence was virtually undetectable in the majority of hematopoietic cells from $Mycn^{M/M}$ adult mice. In contrast to c-Myc–GFP, which is expressed at the highest levels in DN3–4 thymocytes and $Lin^{-}Kit^{+}Sca1^{-}$ bone marrow progenitors, N-myc–mCherry expression was restricted to the most primitive stem and progenitor compartments, such as HSCs and early thymic precursors ($CD4^{-}CD8^{-}CD25^{-}CD44^{hi}Kit^{+}$ ETPs), and tapered off rapidly in more restricted progenitors (Fig. 3c). To assess whether the mCherry fusion could be utilized to faithfully identify cells with differential N-myc protein abundance, HSCs from the bone marrow of $Mycn^{M/M}$ mice were sorted on the basis of mCherry fluorescence (N-myc^{hi} and N-myc^{lo}) and subjected to microarray gene expression profiling. Accordingly, genes upregulated in tumors where N-myc is amplified were significantly enriched in N-myc^{hi} HSCs (Supplementary Fig. 5b,c). In contrast to what we had previously observed in c-Myc^{hi} HSPCs[14], gene signatures associated with adult stem cell populations were enriched in the N-myc^{hi} HSCs (Supplementary Fig. 5d).

Next, we investigated whether HSCs that expressed differential levels of c-Myc or N-myc protein were functionally distinct. To this end, HSC from the bone marrow of $Mycn^{M/M}Myc^{G/G}$ mice were sorted on the intensity of GFP and mCherry fluorescence into four populations (Fig. 3d) and transplanted into lethally irradiated recipients. Recipients transplanted with c-Myc^{hi} HSC (III and IV) had significantly reduced frequency of donor-derived cells in their peripheral blood over time compared to recipients transplanted with c-Myc^{lo} HSC (I and II) (Fig. 3e). This finding agrees with our previous observation that HSPCs expressing higher levels of c-Myc have reduced self-renewal capability[14]. N-myc abundance, on the other hand, was not a clear determinant of stemness, as recipients transplanted with either c-Myc^{lo} N-myc^{hi} (II) or c-Myc^{lo} N-myc^{lo} (I) HSC had equivalent levels of donor chimerism over time. These data suggest that self-renewing HSC preferentially express N-myc and demonstrate that high c-Myc expression can serve as an early indicator of HSC differentiation.

Under stress conditions where HSCs are stimulated to proliferate, c-Myc been found to increase accordingly[28]. To test whether N-myc abundance can respond dynamically to hematopoietic stress, we injected $Mycn^{M/M}Myc^{G/G}$ mice with 5-FU or pI:pC and measured mCherry or GFP fluorescence in HSC 4d later. Since HSCs downregulate c-kit in response to 5-FU treatment, we utilized the SLAM family markers CD48 and CD150 to identify HSCs in 5-FU–treated bone marrow (Fig. 4a). Similarly to c-Myc, we observed a significant

accumulation of N-myc in HSCs from mice treated with either 5-FU or pI:pC (Fig. 4b,c), indicating that N-myc is also upregulated in HSCs as they proliferate in response to stress. This observation led us to hypothesize that depletion of N-myc might impair HSC proliferation in response to 5-FU. Surprisingly, following 5-FU treatment, *Mycn*$^{F/F}$Mx1-Cre^{+} mice had a 2-fold increase in HSC number compared to their wild-type littermates (Fig. 4d). By comparison, loss of *Huwe1* had the opposite effect, severely compromising recovery of the HSC pool after treatment.

Loss of Huwe1 stabilizes N-myc protein in HSCs

To reliably address the impact of *Huwe1* depletion on N-myc stability, we first relied on a well-characterized HSPC-like cell line, HPC-7[29]. Similarly to HSCs, HPC-7 cells can undergo multilineage differentiation, depend on stem cell factor (SCF) for their expansion and express both N-myc and c-Myc (Fig. 5a). HPC-7 cells were transduced with retroviral shRNA constructs targeting either *Huwe1* or *Renilla luciferase* as a negative control. Upon *Huwe1* knockdown, a significant accumulation of N-myc protein, but not c-Myc, was observed (Fig. 5a). We tested several other known Huwe1 substrates, including p53, Miz1 and Mcl1 [17,30,31], but no increase in these proteins was observed. Since Huwe1 has also been implicated in MAP kinase and Wnt signaling[32,33], we also measured phosphorylated Erk1/2 and beta-catenin, yet neither were affected by Huwe1 depletion. To address whether the accumulation of N-myc was proteasome-dependent, the *Huwe1* knockdown study was repeated in the presence of a proteasome inhibitor. Addition of MG-132 significantly stabilized N-myc in cells expressing the control shRNA, while this effect was greatly diminished in cells where Huwe1 was depleted (Fig. 5b). However, p53 was still strongly stabilized in both conditions[34]. Proteins that are polyubiquitylated via lysine 48 (K48) linkage are spared from degradation with MG-132 treatment, implying that there is less ubiquitylated N-myc following *Huwe1* knockdown.

Next, to investigate whether loss of *Huwe1* also results in N-myc accumulation in primary HSCs, we crossed the *Huwe1* conditional knockout mice to the N-myc–mCherry c-Myc–GFP fusion line to generate *Huwe1*$^{F/Y}$Mx1-Cre^{+}*Mycn*$^{M/M}$*Myc*$^{G/G}$ mice. Three weeks after pI:pC treatment, *Huwe1*-deficient HSCs had approximately 3-fold more N-myc protein than wild-type HSCs as determined by mCherrry fluorescence (Fig. 5c,d). We also observed a significant increase in N-myc in *Huwe1*-deficient common myeloid progenitors (CMPs), but not in more lineage-restricted progenitors such as granulocyte-monocyte progenitors (GMPs) (Fig. 5c). In contrast, c-Myc abundance was unchanged in *Huwe1*-deficient HSCs or myeloid progenitors. Taken together with our observations in HPC-7 cells, we can conclude with confidence that *Huwe1* targets N-myc for proteasomal degradation in HSCs.

HSC transcriptional identity disrupted by Huwe1 loss

Since Myc family transcription factors have been shown to bind and influence transcription of a wide distribution of targets, we hypothesized that the stabilization of N-myc occurring in *Huwe1*-deficient HSCs would have profound consequences on gene expression. Thus, we performed high throughput RNA-sequencing on sorted HSCs from wild-type, *Huwe1*$^{F/Y}$Mx1-Cre^{+} and *Huwe1*$^{F/Y}$ *Vav1*-Cre^{+} mice and analyzed transcripts that were differentially expressed (Fig. 6a). 53 genes were significantly upregulated and 224 genes

were significantly downregulated in *Huwe1*-deficient HSC (Supplementary Fig. 6a). Upregulated transcripts included targets of the transcription factor E2F and genes involved in cell cycle progression (Fig. 6b), in agreement with our observation that *Huwe1*-deficient HSCs are more proliferative. Levels of *Stat1* mRNA and interferon-responsive genes were also elevated in *Huwe1*-deficient HSCs (Fig. 6c). Conversely, one of the gene sets most significantly downregulated in *Huwe1*-deficient HSCs pertained to genes that are highly enriched in long-term self-renewing HSCs (Fig. 6b)[35]. These downregulated genes included many critical mediators of HSC quiescence, such as *Mpl*, *Tek* (Tie-2), *Cdkn1c* (p57), *Runx1t1* (Eto) and *Ndn* (necdin)[36–38] (Fig. 6c). Many key effectors of early lymphoid specification, such as *Notch1*, *Gfi1* and *Satb1*[39–41] were also significantly downregulated in the *Huwe1*-deficient HSC.

To address whether these changes in gene expression were due to increased N-myc, we ectopically expressed N-myc in wild-type HSCs and measured several of the differentially expressed transcripts by qRT-PCR. Accordingly, *Mpl, Ndn, Satb1* and *Tek* expression were decreased and *Stat1* increased in HSCs upon enforced N-myc expression (Fig. 6d). To determine which of these genes were direct N-myc targets, we performed chromatin immunoprecipitation followed by deep sequencing (ChIP-seq) to identify regions bound by N-myc in mobilized human $CD34^+$ stem and progenitor cells. Across replicates, we identified 4,466 high-confidence genomic peaks where N-myc was significantly enriched. The largest proportion of peaks were found in gene promoter regions (Supplementary Fig. 6b) and correlated with enrichment of active histone marks, such as H3K27 acetylation and H3K4 trimethylation (Supplementary Fig. 6c), a pattern that has previously been observed for loci bound by c-Myc. Importantly, many of the genes differentially expressed in the *Huwe1*-deficient HSCs were bound by N-myc, such as *STAT1*, *CDK6* and *SATB1* (Fig. 6e). Thus, we conclude that the transcriptional changes observed upon loss of Huwe1 are due, at least in part, to stabilization of N-myc.

Depletion of N-myc in *Huwe1*-deficient mice restores HSC pool

To determine whether the phenotypes of *Huwe1*-deficient HSCs were dependent on N-myc accumulation, $Huwe1^{F/Y}$Mx1-Cre mice were crossed to a *Mycn* conditional knockout line ($Mycn^{F/F}$) to generate *Huwe1/Mycn* double knockout animals (dKO). Unlike their *Huwe1* cKO littermates, aged dKO mice retained a normal population of HSCs in their bone marrow (Fig. 7a,b). Depletion of *Mycn* in *Huwe1*-deficient mice also restored HSC quiescence (Fig. 7c) and serial colony forming ability (Supplementary Fig. 7a). Accordingly, *Cdkn1c, Cdk6 and Stat1* gene expression were restored to normal levels in dKO HSCs (Fig. 7d). Deletion of a single allele of *Mycn* led to a slight, but statistically insignificant increase in phenotypic HSCs in the bone marrow of *Huwe1*–deficient mice (Supplementary Fig. 7b). However, early lymphoid progenitor populations were only minimally rescued in dKO mice (Fig. 7e), suggesting that the loss of lymphoid priming in *Huwe1*-deficient HSCs is largely N-myc independent. Upon transplantation, dKO bone marrow provided long-term myeloid reconstitution in recipient mice to a level comparable to wild-type donors (Fig. 7f), yet lymphoid reconstitution declined over time from both the dKO and *Huwe1* KO donors (data not shown). Unexpectedly, aged mice deficient in *Mycn* alone had nearly a 2-fold increase in HSC compared to their wild-type littermates (Fig. 7b). We did not attribute this effect to

compensation by c-Myc as neither *Myc* mRNA nor protein were increased in *Mycn*-deficient HSCs (Supplementary Fig. 7c,d). To assess whether other known substrates might also account for hematopoietic defects observed in *Huwe1*-deficient mice, Huwe1$^{F/Y}$ HSPCs were simultaneously infected with Cre and shRNA retroviruses and the ability of the doubly-transduced cells to form colonies was measured *in vitro*. shRNA hairpins targeting a panel of previously identified Huwe1 substrates including topoisomerase II binding protein 1 (*Topbp1*), Rev-erbα (*Nr1d1*), p53 (*Trp53*) and *Mycn* [42, 43], were tested in this assay, as well as a control hairpin targeting *Renilla* luciferase. Out of all the constructs tested, only the shRNA targeting *Mycn* could rescue serial colony forming ability in the *Huwe1*-depleted HSPCs (Supplementary Fig. 7e). Altogether, these data propose that *Huwe1* is regulates HSC self-renewal by maintaining homeostatic amounts of N-myc as HSC exit and reenter quiescence.

Discussion

Our findings have uncovered a novel role for the Huwe1 E3 ligase in the maintenance of HSC homeostasis, adding another example of how ubiquitylation and relative abundance of Myc proteins can have a critical role in developmental processes. The observation that Huwe1 can regulate N-myc stability, but not c-Myc, is intriguing given the unspecified function of N-myc in HSCs. Unlike what has been observed in *Myc* conditional knockouts, loss of *Mycn* does not appear to impair adult HSC differentiation[7], but instead leads to an accumulation of HSC in aged mice. However, it remains an open question whether N-myc plays a unique role in fetal or stress hematopoiesis, where we and others have observed a significant enrichment in N-myc expression[44].

An additional provocative discovery described here is the contrast of N-myc and c-Myc protein abundance in HSCs and multipotent progenitors. While others have reported *Myc* and *Mycn* transcripts are co-expressed in the most immature populations of HSCs, this was quantified in a heterogenous population of cells[7]. Utilizing our fluorescent fusions of c-Myc and N-myc, we are now for the first time able to quantify abundance of both proteins at the single-cell level. Instead of uniform co-expression of both proteins in HSC, we observe there are many cells where expression of N-myc and c-Myc was mutually exclusive. Whether or not these cells are functionally unique remains an intriguing possibility. Clearly, from our gene expression analysis of N-myc^{hi} and N-myc^{lo} HSCs there are some distinct molecular differences between these populations, but we found that these populations perform similarly in transplantation assays. Still, the evident switch from N-myc expression in self-renewing, quiescent stem cells to higher c-Myc expression in transit amplifying progenitors has exciting implications for unique functions of Myc family members at the molecular level. Recently, overexpression of *Mycn* was shown to enhance reprogramming of mature blood cells to induced hematopoietic stem cells (iHSCs)[45], suggesting that N-myc, in particular, helps to activate a stem-like identity in hematopoietic cells.

Although there are many similarities between the hematopoietic phenotypes of *Huwe1* and *Fbxw7* conditionally deficient mice, there are some notable differences that might shed light on the role of these ubiquitin ligases in HSCs. Based on our observations in *Huwe1* conditionally deficient mice, we propose that this gradual decline in the HSC pool indicates

a failure to reenter quiescence, as opposed to compulsory cell cycle entry and differentiation, where we would expect a more pronounced phenotype. Hence, in stress scenarios, such as with transplantation or myeloablation, HSC exhausion in *Huwe1*-deficient mice was much more apparent. In steady state, the onset of HSC depletion was considerably slower in *Huwe1*-deficient mice than in *Fbxw7*-deficient mice, and depletion of *Huwe1* in adult mice did not lead to fatal anemia. There are several potential mechanistic explanations why this could be the case. For one, we have observed that both c-Myc and N-myc accumulate in *Fbxw7*-deficient HSC (data not shown), while only N-myc appears to be stabilized upon loss of Huwe1. Therefore, the net sum of Myc proteins would be higher in *Fbxw7*-deficient HSCs and this could result in further amplification of c-Myc and N-myc target gene expression[46]. Alternatively, it is possible that N-myc could be a weaker transcriptional activator than c-Myc. This was hypothesized decades ago[47], but was questioned by the fact that mice harboring homozygous knock-in of *Mycn* into the *Myc* locus develop normally[48]. However, to our knowledge, the effect of equivalently overexpressing either c-Myc or N-myc in HSCs has not been directly compared. Previous studies have also shown that K63-ubiquitylation of c-Myc by Huwe1 can affect its affinity for transcriptional co-activators or Miz-1, a component of a ternary complex with Max found at gene loci that are repressed by c-Myc[18]. If it were also to regulate N-myc in a similar manner, loss of Huwe1 would not only lead to stabilization of N-myc, it would also alter its activity. In support of this notion, we observed more genes are down-regulated in HSCs upon *Huwe1* loss than up-regulated, contrary to what we observe in *Fbxw7*-deficient HSCs.

Finally, if Huwe1 and Fbxw7 are both ubiquitylating the same substrate does this mean that there is a convergence of these two E3 complexes in the same pathway? It is possible that N-myc could be ubiquitylated sequentially or in a concerted fashion by the two E3 complexes. Successive elongation of polyubiquitin chains on protein substrates has been described for RING finger and HECT domain E3 ligases in yeast[49]. It is also possible that the two ligases would act downstream of different signals. Substrate recognition by Fbxw7 depends heavily on the activity of priming kinases (e.g. GSK3β), whereas the events that lead to substrate ubiquitylation by Huwe1 are still poorly defined. it would be intriguing to test whether Huwe1 could still ubiquitylate N-myc with missense substitutions in its phosphodegron or upon inhibition of GSK3β, both of which would block its binding to Fbxw7. In addition to Huwe1 and Fbxw7, there are several other E3 ligases that have been shown to regulate ubiquitylation of Myc proteins[50] and it is only through these sort of genetic and biochemical studies that we can begin to unravel the complex interplay of these proteins in HSCs.

METHODS

Mice

Huwe1 and *Mycn* conditional knockout (floxed) mice, as well as the *Myc*^{GFP} knock-in allele have been described previously[19, 26, 51]. To delete gene loci specifically in the hematopoietic system, conditional knockout lines were crossed to *Mx1*-Cre and *Vav1*-Cre transgenic lines[24, 52]. *Mx1*-Cre was induced by three consecutive intraperitoneal injections of poly(I)·poly(C) (GE Healthcare, 10 mg/kg) administered every other day. 5-fluorouracil powder (Sigma-Aldrich) was dissolved in PBS at a concentration of 10 mg/ml and administered by

intraperitoneal injection at a dose of 150 mg/kg. For transplant studies, congenic CD45.1$^+$ recipients (B6.SJL-Ptprc^a) were exposed to 12 Gy of gamma irradiation (administered in two doses, 4 h apart) and cells were transferred intravenously by retroorbital injection. For transplant of sorted populations, 2×10^5 unfractionated CD45.1$^+$ bone marrow cells were added for hemogenic support. Peripheral blood was sampled periodically from experimental and control mice and blood counts were determined by Hemavet analysis (Drew Scientific).

To generate the *Mycn* mCherry fusion (*Mycn*^{M}) allele, an 8.88 kb genomic DNA fragment was subcloned from a positively identified 129SvEv BAC clone (RP22: 127D5). An mCherry coding sequence was PCR amplified and subcloned into a recombineered SalI site within targeting vector just after the ATG start codon within *Mycn* exon 2. A pGK-gb2-*lox*P-*neo*^{r} cassette was inserted 550 bp downstream of exon 2. The long homology arm extended 5.6 kb 5′ of the mCherry sequence and the short homology arm extended 2 kb downstream of the *neo*^{r} cassette. The resulting targeting vector was linearized with NotI and electroporated into W4 129S6/SVEvTac ES cells. Neomycin-resistant clones were screened by short arm PCR and injected into C57BL/6 EIIA-Cre blastocysts to remove the *neo*^{r} cassette from the germline[53]. Genotyping of pups following backcross to wild-type C57BL/6 mice was performed by PCR using the following primers: *Mycn*_F: 5′-TTGGCTCATTCTCTCTTGGTTTGC-3′, *Mycn*_R: 5′-AGCATCTCCGTAGCCCAATTCG-3′, mCherry_R: 5′-GCCGTCCTCGAAGTTCATCA-3′. All animal experiments were done in accordance to the guidelines of the NYU School of Medicine or Institutional Animal Care and Use Committee.

Flow cytometry

Single-cell suspensions were derived from mechanical disruption of mouse bone marrow, spleen, thymus and fetal liver in PBS supplemented with 2% fetal calf serum (FCS, Sigma). For FACS analysis of spleen, fetal liver and peripheral blood, red blood cells were lysed with ACK buffer. Nonspecific antibody binding was blocked by incubation with 20 μg/ml Rat IgG (Sigma) for 15 min. Cells were incubated with primary antibodies for 45 min and streptavidin conjugates, when applicable, for 15 min on ice. The antibodies used in this study are listed in Supplementary Table 1. Lineage-negative cells were defined by lack of expression of Gr-1, TER-119, CD4, CD8, B220 and CD11b (except for fetal liver samples). For intracellular Ki67 and DAPI staining in HSC, following staining of surface antigens, bone marrow cells were fixed with 4% paraformaldehyde and permeabilized with 0.1% saponin prior to addition of anti-Ki67 (BD Biosciences) and 2 μg/ml DAPI. For sorting of rare HSC populations, bone marrow was enriched for stem and progenitor cells via magnetic selection with anti-CD117 microbeads (Miltenyi Biotec) prior to antibody staining and sorting. Stained cells were quantified using a BD Fortessa analyzer or isolated with a BD ARIA II. FlowJo software (Treestar) was used to generate flow cytometry plots, histograms and calculate mean fluorescence intensities.

Immunoblots

Whole cell extracts were prepared by resuspending cells in RIPA buffer (50 mM Tris-HCl pH 8, 150 mM NaCl, 1% NP-40 substitute, 0.5% sodium deoxycholate, 0.1% SDS)

supplemented with complete protease inhibitor cocktail (Roche). Cleared lysates were boiled in Laemmli sample buffer with 1% beta-mercaptoethanol and proteins were separated by SDS-PAGE using precast 4–12% Bis-Tris gels (Life Technologies). Proteins were transferred to PVDF membrane (Millipore) at 30 V, 4 °C for 16 h. Blots were blocked for 30 min with 5% milk in TBS-T, incubated with primary antibodies for >3h and horseradish peroxidase conjugated anti-mouse IgG or anti-rabbit IgG (GE Healthcare) for 1 h, washing 4× for 10 min with excess TBS-T in between and prior to developing. Blots were developed with SuperSignal West Pico ECL substrate (Thermo Scientific) and exposed to film. The following antibodies were used in this study: Huwe1 (Bethyl, A300–486A, 1:1000), N-myc (Santa Cruz, B8.4.B, 1:500), c-Myc (Cell Signaling, 9402, 1:500), Mcl-1 (Santa Cruz, S-19, 1:200), Miz-1 (Santa Cruz, H-190, 1:200), beta catenin (Cell Signaling, 8480, 1:1000), Erk1/2 (Cell Signaling, 4695, 1:1000), phospo-Erk1/2 (Cell Signaling, D13.14.4E, 1:1000), p53 (Leica, CM5, 1:1000), vinculin (Sigma, hVIN-1, 1:5000) and actin (EMD Millipore, C4, 1:5000).

Cell culture

Murine ESCs were grown as previously described[14]. HPC-7 cells were grown in IMDM (Gibco) supplemented with 5% FCS, 100 ng/ml SCF (Peprotech), 100 U/ml penicillin-streptomycin (Cellgro), and 150 μM 1-thioglycerol (Sigma). Primary sorted HSCs were cultured in Opti-MEM with 10% FCS, 55 μM beta-mercaptoethanol (Gibco), 100 U/ml penicillin-streptomycin, 100 ng/ml SCF and 20 ng/ml Tpo (Peprotech) in 96-well round bottom plates at a density of 0.5–1 × 10^4/well. Differentiation of HSPCs to B and T lymphocytes on OP9 stroma was performed as described[54]. Retrovirus was produced by transfecting Plat-E cells with MSCV vectors and collecting supernatant 48 h and 72 h later. Viral supernatant was passed through a 0.45 μm syringe filter (Corning) and concentrated with Amicon 100 kDa centrifugal filters (Millipore). HPC-7 cells and primary HSC were infected by addition of concentrated virus in the presence of 4 μg/ml polybrene and centrifuged at 800 x g for 90 min at 30 °C. Antibiotic-resistance selection of cells was achieved by addition of 2 μg/ml puromycin or 500 μg/ml G418. MG-132 (Z-Leu-Leu-Leu-H aldehyde, Peptides International) was dissolved in DMSO and added to cultueres at a final concentration of 10 μM. For colony forming assays, 200 sorted HSPCs were plated in triplicate in 3-cm dishes with 1 ml M3434 media (StemCell Technologies). After 7 d, colonies were scored, harvested and serially replated at 5 × 10^3 cells/dish.

High throughput RNA sequencing and microarray analysis

Cell populations were sorted directly into Trizol reagent (Life Technologies). Nucleic acids were extracted according to manufacturer instructions and precipitated in isopropanol with glycogen or linear acrylamide (Ambion) used as a carrier. After 30 min of DNase I treatment (Life Technologies), RNA was purified with RNA clean and concentrator columns (Zymo). RNA integrity was verified on a Agilent 2100 Bioanalyzer Pico chip. For small-scale RNA sequencing, full-length cDNA libraries were prepared using the SMARTer Ultra Low Input RNA kit (Clontech). Amplified cDNA libraries were sheared to 200–500 bp fragments using a Covaris LE220. End repair, A-tailing and Illumina adaptor ligation reactions were carried out using a NEBNext Library Prep Kit (New England BioLabs). Libraries were sequenced on an Illumina HiSeq2500 v4 using 50-bp paired-end reads. Fastq files were aligned to mm9

using TopHat allowing 2 mismatches. Aligned features were sorted with samtools, counted with htseq-count and differential expression was determined using the 'edgeR' package in Bioconductor, as described[55]. Microarray gene expression profiling of sorted N-myc^{hi} and N-myc^{lo} HSC and GSEA was carried out as previously described[27]. Heat map representations of row mean centered expression values were generated using the 'pheatmap' package in Bioconductor.

ChIP-sequencing

For the analysis of N-Myc binding, 3×10^7 human CD34$^+$ cells were fixed in 1% formaldehyde for 10 min at 37°C, then lysed by the addition of lysis buffer 1 (5 mM PIPES pH 8, 85 mM KCl, 0,5% NP40) and incubated for 20 min at 4°C. The cells were then pelleted and resuspended in lysis buffer 2 (10 mM Tris/HCl pH 7.5, 150 mM NaCl, 1 mM EDTA, 1% NP-40, 1% deoxycholic acid sodium salt, 0.1% SDS) and incubated for 10 min at 4 °C. Nuclei were sonicated using a Bioruptor (Diagenode). 3 μg of N-myc antibody (B8.4.B, Santa Cruz) was coupled to 30 μl of Dynabeads (A/G-mixture) overnight and the complex was added to chromatin followed by a 6 h incubation at 4 °C with rotation. Complexes bound to the beads were washed three times with wash buffer A (20 mM Tris-HCl pH 8.1, 150 mM NaCl, 2 mM EDTA, 0.1% SDS, 1% Triton X-100), three times with wash buffer B (20 mM Tris-HCl pH 8.1, 500 mM NaCl, 2 mM EDTA, 0.1% SDS, 1% Triton X-100) and three times with wash buffer C (10 mM Tris-HCl pH 8.1, 250 mM LiCl, 1 mM EDTA, 1% NP-40 and 1% sodium deoxycholate). Beads were eluted twice with elutuion buffer (1% SDS, 0.1 M $NaHCO_3$) incubating for 15 min each time followed by treatment with RNAseA (20 μg/ml) and proteinase K (200 μg/ml). DNA was purified by phenol-chloroform extraction and resuspended in TE buffer. ChIP-seq libraries were generated: end repair, A-tailing, adaptor ligation (Illumina TruSeq system) and PCR amplification. AMPure XP beads (Beckman Coulter, A63880) were used for DNA cleaning in each step of the process. Raw images generated by Illumina HiSeq2000 using the default set of parameters were processed by CASAVA to remove the first and last bases and then they were used to generate sequence reads in fastq format.

Reads were aligned to hg19 human genome using Bowtie2[56] with the standard parameters (except for –m 1 in order to report only unique alignments). MACS version 2.0.10[57] was used to perform peak calling for both broad and narrow peaks. The files with the aligned reads were converted to wig format using GenomicTools[58] and then to bigwig format using the corresponding UCSC tool (wigToBigWig, UCSC Browser binary utilities) in order to visualize the tracks. Snapshots were prepared using the Integrative Genomics Viewer (IGV). GEO Datasets GSM537652 and GSM772885 were used to determine histone modifications occupancy in human CD34$^+$ cells. DeepTools[59] was used to generate heatmap visualizations.

Quantitative real-time PCR

RNA was extracted from sorted populations as described for RNA sequencing. cDNA was prepared using the High-Capacity RNA-to-DNA Kit (Applied Biosystems). Real time PCR reactions were carried out using SYBR Green Master Mix (Roche) and run on a Lightcycler 480 II (Roche). Relative mRNA abundance between samples was calculated with the $\Delta\Delta C_T$

method using *Gapdh* as an internal control. The specific primer sequences used for qRT-PCR in this study are listed in Supplementary Table 2.

Histology

Tissues were dissected from mice and fixed overnight in 10% buffered formalin (Fisher Scientific). Spleens were dehydrated in ethanol and embedded in paraffin for sectioning. Bones were decalcified in 0.5 M EDTA for 48 h prior to dehydration and embedding. 5 μm paraffin sections were stained with hematoxylin and eosin for brightfield microscopy. Peripheral blood smears were briefly fixed in methanol, stained with Wright-Giemsa solution (Protocol, Fisher Scientific) and mounted in Cytoseal 60 (Thermo). Images were taken using a Zeiss Axio Observer microscope.

Statistical analysis

Statistical analyses were performed using GraphPad Prism or R. We calculated whether data points were normally distributed using the Kolmogorov-Smirnov test. When two groups were compared, a two-tailed *t*-test with Welch's correction or Mann-Whitney test was used. When several groups were compared, a one-way ANOVA test followed by Dunnet's test for multiple comparisons was used. $P \leq 0.05$ was considered significant.

Supplementary Material

Refer to Web version on PubMed Central for supplementary material.

Acknowledgments

We would like to thank the members of the Aifantis laboratory for helpful discussions. Also, we thank A. Heguy and members of the NYU Genome Technology Center, for expert assistance RNA sequencing, the NYU Flow Cytometry facility for expert cell sorting and the NYU Histology Core. We would also like to thank G. Inghirami from Weill Cornell Medicine for assistance with histopathological evaluations. We thank S. Heimfeld at Fred Hutchinson Cancer Research Center for providing human $CD34^+$ cells (Core Center of Excellence NIDDK Grant # DK56465). The Aifantis Lab is supported by National Institutes of Health (1R01CA169784, 1R01CA133379, 1R01CA105129, 1R01CA149655, 5R01CA173636), the William Lawrence and Blanche Hughes Foundation, The Leukemia & Lymphoma Society (TRP#6340-11, LLS#6373-13), The Chemotherapy Foundation, The V Foundation for Cancer Research, the Alex's Lemonade Stand Foundation for Childhood Cancer and the St. Baldrick's Cancer Research Foundation. B.K. is the Berger Foundation Fellow of the Damon Runyon Cancer Research Foundation (DRG-2234-15). This work was also supported by a grant from the Deutsche Forschungsgemeinschaft to E.W. (Emmy Noether Research Group, WO 2108/1-1) and by an American-Italian Cancer Foundation Post-Doctoral Research Fellowship to F. Boccalatte.

References

1. Schuettpelz L, Link D. Regulation of hematopoietic stem cell activity by inflammation. Front. Immunol. 2013; 4:204. [PubMed: 23882270]
2. Pietras E, Warr M, Passegué E. Cell cycle regulation in hematopoietic stem cells. J. Cell Biol. 2011; 195(5):709–720. [PubMed: 22123859]
3. Rossi L, Lin KK, Boles NC, Yang L, King KY, Jeong M, et al. Less is more: unveiling the functional core of hematopoietic stem cells through knockout mice. Cell Stem Cell. 2012; 11(3):302–317. [PubMed: 22958929]
4. Wang R, Dillon C, Shi L, Milasta S, Carter R, Finkelstein D, et al. The transcription factor Myc controls metabolic reprogramming upon T lymphocyte activation. Immunity. 2011; 35(6):871–882. [PubMed: 22195744]

5. Dang C. c-Myc target genes involved in cell growth, apoptosis, and metabolism. Mol. Cell. Biol. 1999; 19(1):1–11. [PubMed: 9858526]
6. Scognamiglio R, Cabezas-Wallscheid N, Thier MC, Altamura S, Reyes A, Prendergast AM, et al. Myc Depletion Induces a Pluripotent Dormant State Mimicking Diapause. Cell. 2016; 164(4):668–680. [PubMed: 26871632]
7. Laurenti E, Varnum-Finney B, Wilson A, Ferrero I, Blanco-Bose W, Ehninger A, et al. Hematopoietic stem cell function and survival depend on c-Myc and N-Myc activity. Cell Stem Cell. 2008; 3(6):611–624. [PubMed: 19041778]
8. Wilson A, Murphy M, Oskarsson T, Kaloulis K, Bettess M, Oser G, et al. c-Myc controls the balance between hematopoietic stem cell self-renewal and differentiation. Genes Dev. 2004; 18(22): 2747–2763. [PubMed: 15545632]
9. Sears R, Nuckolls F, Haura E, Taya Y, Tamai K, Nevins J. Multiple Ras-dependent phosphorylation pathways regulate Myc protein stability. Genes Dev. 2000; 14(19):2501–2514. [PubMed: 11018017]
10. Lutterbach B, Hann S. Hierarchical phosphorylation at N-terminal transformation-sensitive sites in c-Myc protein is regulated by mitogens and in mitosis. Mol. Cell. Biol. 1994; 14(8):5510–5522. [PubMed: 8035827]
11. Sjostrom S, Finn G, Hahn W, Rowitch D, Kenney A. The Cdk1 complex plays a prime role in regulating N-myc phosphorylation and turnover in neural precursors. Dev. Cell. 2005; 9(3):327–338. [PubMed: 16139224]
12. Gregory M, Qi Y, Hann S. Phosphorylation by glycogen synthase kinase-3 controls c-myc proteolysis and subnuclear localization. J. Biol. Chem. 2003; 278(51):51606–51612. [PubMed: 14563837]
13. Welcker M, Orian A, Jin J, Grim J, Grim J, Harper J, et al. The Fbw7 tumor suppressor regulates glycogen synthase kinase 3 phosphorylation-dependent c-Myc protein degradation. Proc. Natl. Acad. Sci. USA. 2004; 101(24):9085–9090. [PubMed: 15150404]
14. Reavie L, Della Gatta G, Crusio K, Aranda-Orgilles B, Buckley SM, Thompson B, et al. Regulation of hematopoietic stem cell differentiation by a single ubiquitin ligase-substrate complex. Nat. Immunol. 2010; 11(3):207–215. [PubMed: 20081848]
15. Thompson B, Jankovic V, Gao J, Buonamici S, Vest A, Lee J, et al. Control of hematopoietic stem cell quiescence by the E3 ubiquitin ligase Fbw7. J. Exp. Med. 2008; 205(6):1395–1408. [PubMed: 18474632]
16. Matsuoka S, Oike Y, Onoyama I, Iwama A, Arai F, Takubo K, et al. Fbxw7 acts as a critical fail-safe against premature loss of hematopoietic stem cells and development of T-ALL. Genes Dev. 2008; 22(8):986–991. [PubMed: 18367647]
17. Zhong Q, Gao W, Du F, Wang X. Mule/ARF-BP1, a BH3-only E3 ubiquitin ligase, catalyzes the polyubiquitination of Mcl-1 and regulates apoptosis. Cell. 2005; 121(7):1085–1095. [PubMed: 15989957]
18. Adhikary S, Marinoni F, Hock A, Hulleman E, Popov N, Beier R, et al. The ubiquitin ligase HectH9 regulates transcriptional activation by Myc and is essential for tumor cell proliferation. Cell. 2005; 123(3):409–421. [PubMed: 16269333]
19. Zhao X, Heng J, Guardavaccaro D, Jiang R, Pagano M, Guillemot F, et al. The HECT-domain ubiquitin ligase Huwe1 controls neural differentiation and proliferation by destabilizing the N-Myc oncoprotein. Nat. Cell Biol. 2008; 10(6):643–653. [PubMed: 18488021]
20. Zhao X, D Arca D, Lim WK, Brahmachary M, Carro MS, Ludwig T, et al. The N-Myc-DLL3 Cascade Is Suppressed by the Ubiquitin Ligase Huwe1 to Inhibit Proliferation and Promote Neurogenesis in the Developing Brain. Dev. Cell. 2009; 17
21. Lara-Astiaso D, Weiner A, Lorenzo-Vivas E, Zaretsky I, Jaitin D, David E, et al. Immunogenetics. Chromatin state dynamics during blood formation. Science. 2014; 345(6199):943–949. [PubMed: 25103404]
22. Van Zant G. Studies of hematopoietic stem cells spared by 5-fluorouracil. J. Exp. Med. 1984; 159(3):679–690. [PubMed: 6699542]
23. Essers M, Offner S, Blanco-Bose W, Waibler Z, Kalinke U, Duchosal M, et al. IFNalpha activates dormant haematopoietic stem cells in vivo. Nature. 2009; 458(7240):904–908. [PubMed: 19212321]

24. Stadtfeld M, Graf T. Assessing the role of hematopoietic plasticity for endothelial and hepatocyte development by non-invasive lineage tracing. Development. 2004; 132(1):203–213. [PubMed: 15576407]
25. Kondo M. Lymphoid and myeloid lineage commitment in multipotent hematopoietic progenitors. Immunol. Rev. 2010; 238(1):37–46. [PubMed: 20969583]
26. Huang CY, Bredemeyer AL, Walker LM, Bassing CH, Sleckman BP. Dynamic regulation of c-Myc proto-oncogene expression during lymphocyte development revealed by a GFP-c-Myc knock-in mouse. Eur. J. Immunol. 2008; 38(2):342–349. [PubMed: 18196519]
27. King B, Trimarchi T, Reavie L, Xu L, Mullenders J, Ntziachristos P, et al. The ubiquitin ligase FBXW7 modulates leukemia-initiating cell activity by regulating MYC stability. Cell. 2013; 153(7):1552–1566. [PubMed: 23791182]
28. Ehninger A, Boch T, Uckelmann H, Essers M, Müdder K, Sleckman B, et al. Posttranscriptional regulation of c-Myc expression in adult murine HSCs during homeostasis and interferon-α-induced stress response. Blood. 2014; 123(25):3909–3913. [PubMed: 24795346]
29. Pinto do OP, Kolterud A, Carlsson L. Expression of the LIM-homeobox gene LH2 generates immortalized steel factor-dependent multipotent hematopoietic precursors. EMBO J. 1998; 17(19): 5744–5756. [PubMed: 9755174]
30. Hao Z, Duncan GS, Su YW, Li WY, Silvester J, Hong C, et al. The E3 ubiquitin ligase Mule acts through the ATM-p53 axis to maintain B lymphocyte homeostasis. J. Exp. Med. 2012; 209(1): 173–186. [PubMed: 22213803]
31. Inoue S, Hao Z, Elia AJ, Cescon D, Zhou L, Silvester J, et al. Mule/Huwe1/Arf-BP1 suppresses Ras-driven tumorigenesis by preventing c-Myc/Miz1-mediated down-regulation of p21 and p15. Genes Dev. 2013; 27(10):1101–1114. [PubMed: 23699408]
32. Jang ER, Shi P, Bryant J, Chen J, Dukhande V, Gentry MS, et al. HUWE1 is a molecular link controlling RAF-1 activity supported by the Shoc2 scaffold. Mol. Cell. Biol. 2014; 34(19):3579–3593. [PubMed: 25022756]
33. de Groot RE, Ganji RS, Bernatik O, Lloyd-Lewis B, Seipel K, Sedova K, et al. Huwe1-mediated ubiquitylation of dishevelled defines a negative feedback loop in the Wnt signaling pathway. Sci Signal. 2014; 7(317) ra26.
34. Chen D, Kon N, Li M, Zhang W, Qin J, Gu W. ARF-BP1/Mule is a critical mediator of the ARF tumor suppressor. Cell. 2005; 121(7):1071–1083. [PubMed: 15989956]
35. Ivanova N, Dimos J, Schaniel C, Hackney J, Moore K, Lemischka I. A stem cell molecular signature. Science. 2002; 298(5593):601–604. [PubMed: 12228721]
36. Tesio M, Trumpp A. Breaking the cell cycle of HSCs by p57 and friends. Cell Stem Cell. 2011; 9(3):187–192. [PubMed: 21885016]
37. Liu Y, Elf S, Miyata Y, Sashida G, Liu Y, Huang G, et al. p53 regulates hematopoietic stem cell quiescence. Cell Stem Cell. 2009; 4(1):37–48. [PubMed: 19128791]
38. de Graaf CA, Metcalf D. Thrombopoietin and hematopoietic stem cells. Cell Cycle. 2011; 10(10): 1582–1589. [PubMed: 21478671]
39. Phelan J, Saba I, Zeng H, Kosan C, Messer M, Olsson H, et al. Growth factor independent-1 maintains Notch1-dependent transcriptional programming of lymphoid precursors. PLoS Genet. 2013; 9(9)
40. Satoh Y, Yokota T, Sudo T, Kondo M, Lai A, Kincade P, et al. The Satb1 protein directs hematopoietic stem cell differentiation toward lymphoid lineages. Immunity. 2013; 38(6):1105–1115. [PubMed: 23791645]
41. Ye M, Graf T. Early decisions in lymphoid development. Curr. Opin. Immunol. 2007; 19(2):123–128. [PubMed: 17306518]
42. Yin L, Joshi S, Wu N, Tong X, Lazar M. E3 ligases Arf-bp1 and Pam mediate lithium-stimulated degradation of the circadian heme receptor Rev-erb alpha. Proc. Natl. Acad. Sci. USA. 2010; 107(25):11614–11619. [PubMed: 20534529]
43. Herold S, Hock A, Herkert B, Berns K, Mullenders J, Beijersbergen R, et al. Miz1 and HectH9 regulate the stability of the checkpoint protein, TopBP1. EMBO J. 2008; 27(21):2851–2861. [PubMed: 18923429]

44. Ye M, Zhang H, Amabile G, Yang H, Staber P, Zhang P, et al. C/EBPa controls acquisition and maintenance of adult haematopoietic stem cell quiescence. Nat. Cell Biol. 2013; 15(4):385–394. [PubMed: 23502316]
45. Riddell J, Gazit R, Garrison BS, Guo G, Saadatpour A, Mandal PK, et al. Reprogramming committed murine blood cells to induced hematopoietic stem cells with defined factors. Cell. 2014; 157(3):549–564. [PubMed: 24766805]
46. Lin CY, Loven J, Rahl PB, Paranal RM, Burge CB, Bradner JE, et al. Transcriptional Amplification in Tumor Cells with Elevated c-Myc. Cell. 2012; 151(1):56–67. [PubMed: 23021215]
47. Barrett J, Birrer M, Kato G, Dosaka-Akita H, Dang C. Activation domains of L-Myc and c-Myc determine their transforming potencies in rat embryo cells. Mol. Cell. Biol. 1992; 12(7):3130–3137. [PubMed: 1620120]
48. Malynn B, de Alboran I, O'Hagan R, Bronson R, Davidson L, DePinho R, et al. N-myc can functionally replace c-myc in murine development, cellular growth, and differentiation. Genes Dev. 2000; 14(11):1390–1399. [PubMed: 10837031]
49. Metzger M, Weissman A. Working on a chain: E3s ganging up for ubiquitylation. Nat. Cell Biol. 2010; 12(12):1124–1126. [PubMed: 21124306]
50. Farrell AS, Sears RC. MYC degradation. Cold Spring Harb Perspect Med. 2014; 4(3)

Methods only references

51. Knoepfler P, Cheng P, Eisenman R. N-myc is essential during neurogenesis for the rapid expansion of progenitor cell populations and the inhibition of neuronal differentiation. Genes Dev. 2002; 16(20):2699–2712. [PubMed: 12381668]
52. Kühn R, Schwenk F, Aguet M, Rajewsky K. Inducible gene targeting in mice. Science. 1995; 269(5229):1427–1429. [PubMed: 7660125]
53. Lakso M, Pichel JG, Gorman JR, Sauer B, Okamoto Y, Lee E, et al. Efficient in vivo manipulation of mouse genomic sequences at the zygote stage. Proc. Natl. Acad. Sci. USA. 1996; 93(12):5860–5865. [PubMed: 8650183]
54. Holmes R, Zúñiga-Pflücker JC. The OP9-DL1 system: generation of T-lymphocytes from embryonic or hematopoietic stem cells in vitro. Cold Spring Harbor protocols. 2009; 2009(2)
55. Anders S, McCarthy DJ, Chen Y, Okoniewski M, Smyth GK, Huber W, et al. Count-based differential expression analysis of RNA sequencing data using R and Bioconductor. Nature protocols. 2013; 8(9):1765–1786. [PubMed: 23975260]
56. Langmead B, Salzberg SL. Fast gapped-read alignment with Bowtie 2. Nat. Methods. 2012; 9(4): 357–359. [PubMed: 22388286]
57. Zhang Y, Liu T, Meyer CA, Eeckhoute J, Johnson DS, Bernstein BE, et al. Model-based analysis of ChIP-Seq (MACS). Genome Biol. 2008; 9(9):R137. [PubMed: 18798982]
58. Tsirigos A, Haiminen N, Bilal E, Utro F. GenomicTools: a computational platform for developing high-throughput analytics in genomics. Bioinformatics. 2012; 28(2):282–283. [PubMed: 22113082]
59. Ramirez F, Dundar F, Diehl S, Gruning BA, Manke T. deepTools: a flexible platform for exploring deep-sequencing data. Nucleic Acids Res. 2014; 42(Web Server issue):W187–W191. [PubMed: 24799436]

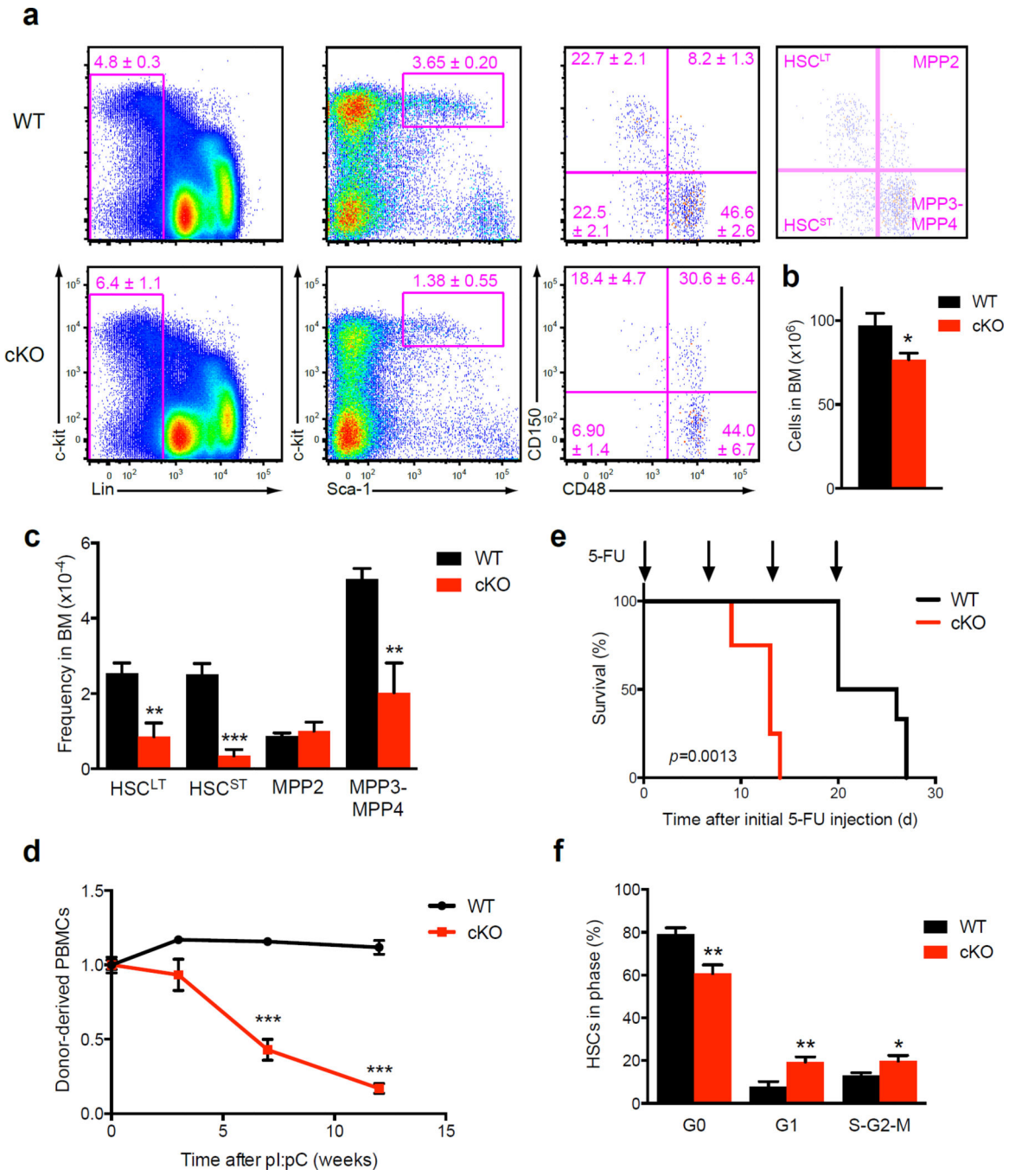

Figure 1. *Huwe1* is essential for HSC self-renewal and quiescence

(**a**) Flow cytometry and total cell counts (**b**) of bone marrow from *Huwe1*$^{+/Y}$ Mx1-Cre^{+} (WT) ($n = 11$) or *Huwe1*$^{F/Y}$ Mx1-Cre^{+} (cKO) ($n = 8$) mice analyzed 4 months after pI:pC treatment. Gate frequencies show mean percentage of parent gate ± s.e.m. (**c**) Frequencies of stem and multipotent progenitor populations in bone marrow of mice analyzed in (**a**). (**d**) Ratio of donor chimerism in peripheral blood of recipient mice that were transplanted with bone marrow from either *Huwe1*$^{+/Y}$ Mx1-Cre^{+} ($n = 3$) or *Huwe1*$^{F/Y}$ Mx1-Cre^{+} ($n = 8$) (CD45.2) mixed 1:1 with wild-type (CD45.1) competitor. Ratio of CD45.2^{+} to CD45.1^{+}

cells in peripheral blood of recipients after pI:pC treatment is plotted over time. (**e**) Kaplan-Meier curve plotting survival of WT ($n = 6$) or cKO ($n = 4$) mice injected weekly with 150mg/kg 5-fluorouracil i.p. (**f**) Cell cycle status of HSC in WT ($n = 5$) or cKO ($n = 5$) mice as determined by Ki67/DAPI staining. *$P < 0.05$, **$P < 0.01$, ***$P < 0.001$ (two-tailed *t*-test). Data are from three experiments (**a-c, f**; mean and s.e.m), representative of two experiments (**d**; mean and s.e.m.) or one experiment (**e**; Mantel-Cox Log Rank test, median survival 12d vs. 20d, $P = 0.0069$).

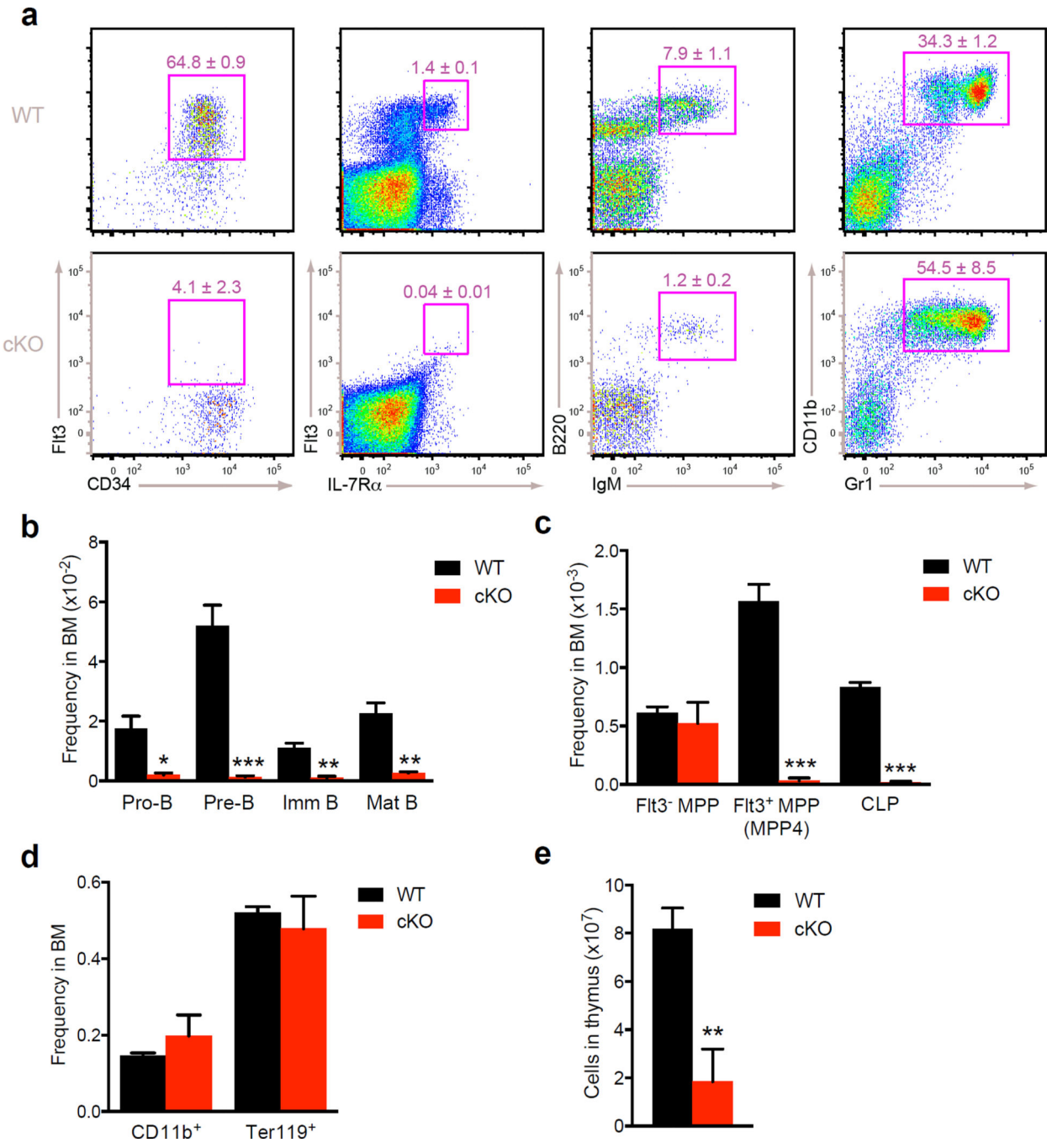

Figure 2. Lymphoid specification is impaired in *Huwe1*-deficient HSC

(**a**) FACS analysis of bone marrow from 8-week-old *Huwe1*$^{+/Y}$ Vav1-Cre^{+} (WT) ($n = 4$) or *Huwe1*$^{F/Y}$ Vav1-Cre^{+} (cKO) ($n = 4$) mice. Gate frequencies show mean percentage of parent gate ± s.e.m. Overall frequencies of developing and mature B cells (**b**), lineage-primed multipotent progenitors (**c**) and mature myeloid cells or erythroid precursors (**d**) in bone marrow of these mice are plotted. (**f**) Cell counts of thymii isolated from 8-week-old WT or cKO mice. *$P < 0.05$, **$P < 0.01$, ***$P < 0.001$ (two-tailed *t*-test). Data are representative of two experiments (mean and s.e.m. in **b-e**).

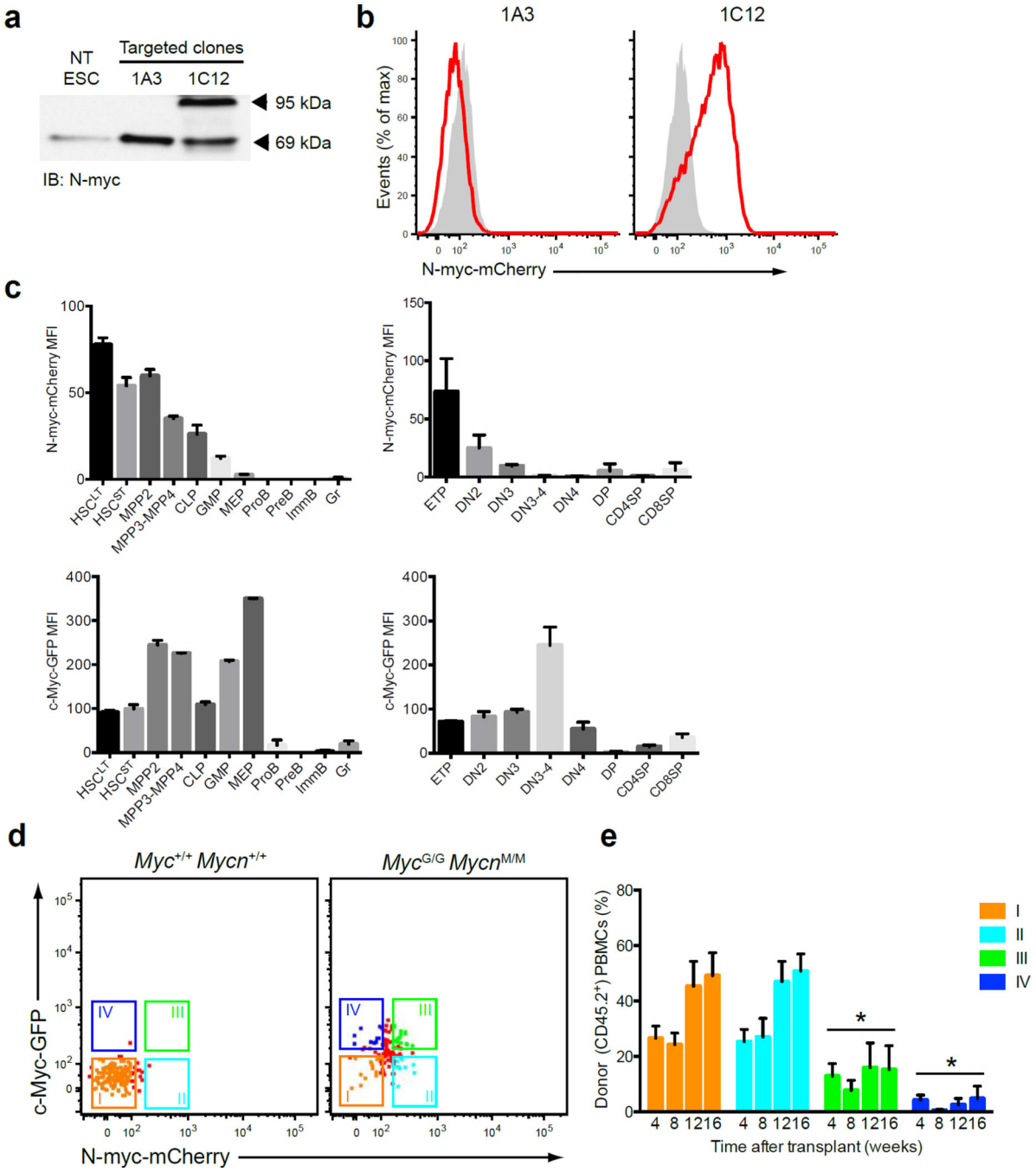

Figure 3. Generation of an mCherry fusion allele to measure N-myc protein abundance in single hematopoietic cells

(**a**) Immunoblot of lysates from control (NT) and two neomycin-resistant, targeted ESC clones that were infected with a retrovirus to express Cre recombinase, probed with anti-N-myc antibody. (**b**) FACS histogram measuring mCherry fluorescence of targeted, Cre-infected ESC clones from (**a**). mCherry fluorescence in NT ESC is shown in solid grey for reference. (**c**) N-myc and c-Myc abundance in hematopoietic populations in bone marrow and thymus of $Mycn^{M/M}Myc^{G/G}$ mice, as determined by mean mCherry or GFP

fluorescence intensity. (**d**) HSCs from bone marrow of *Mycn*$^{M/M}$*Myc*$^{G/G}$ were sorted into 4 populations (I-IV) on the basis of GFP and mCherry fluorescence. HSCs from *Mycn*$^{+/+}$*Myc*$^{+/+}$ mice were used as a control to determine gates. (**e**) 200 cells from each population were transplanted into lethally irradiated recipients and donor chimerism in peripheral blood (CD45.2^{+}) was measured over time. *$P < 0.05$ (one-way ANOVA). Data are representative of two experiments (**a-b**), two experiments with three biological replicates each (**c**; mean and s.e.m.), or two experiments with five recipients per group (**e**; mean and s.e.m.).

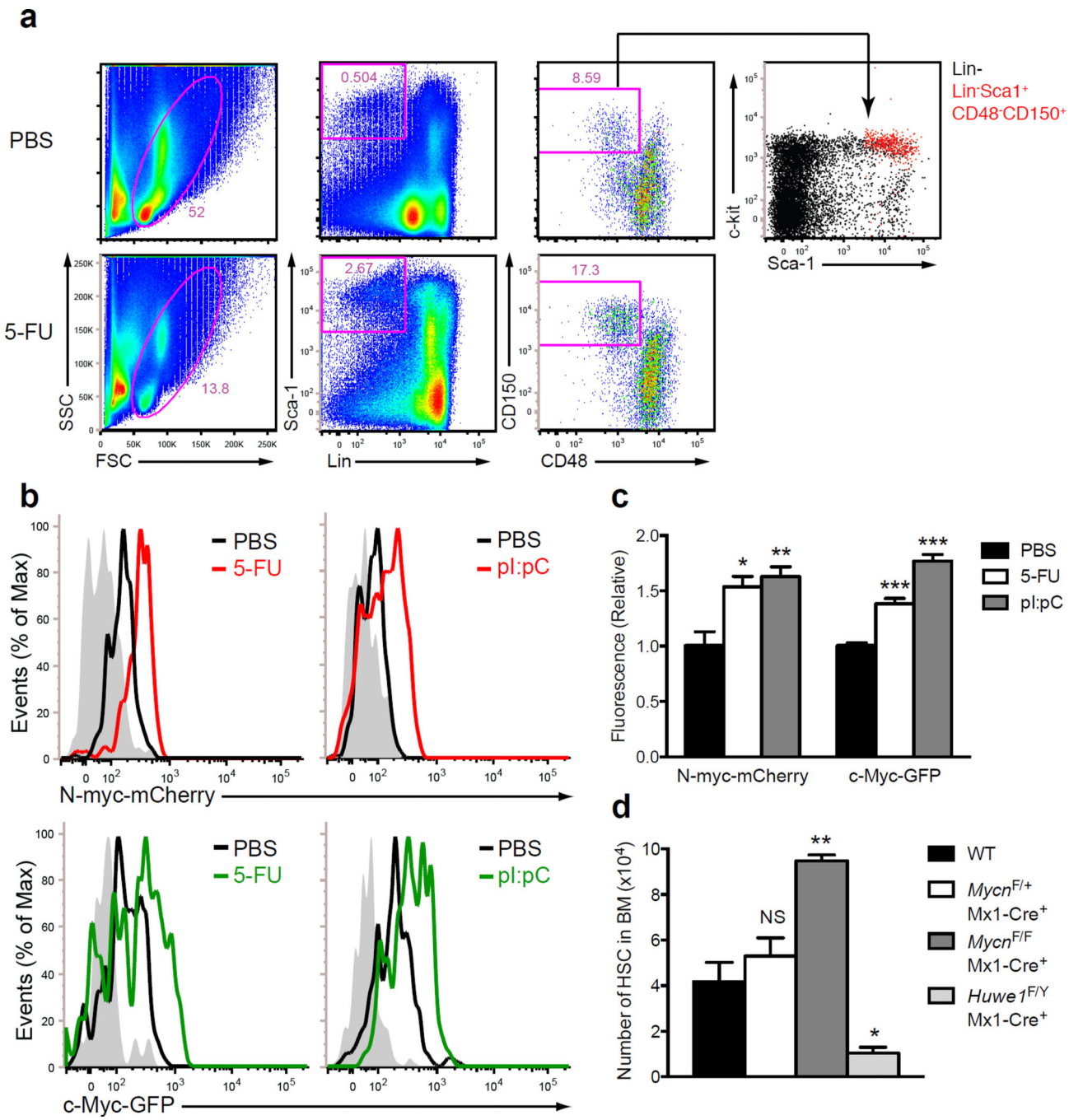

Figure 4. N-myc protein abundance in HSCs increases in response to stress

Mycn$^{M/M}$*Myc*$^{G/G}$ mice were injected with 5-FU (150mg/kg i.p. 1x), pI:pC (10mg/kg i.p. 2x) or PBS and their bone marrow was isolated and analyzed by 4d later. (**a**) Gating strategy for identifying HSC in bone marrow of 5-FU treated mice. Overlay shows that the majority of Lin^{-}Sca1^{+}CD48^{-}CD150^{+} bone marrow cells are c-kit+ in PBS-injected mice. (**b**) FACS histogram comparing mCherry and GFP fluorescence in HSC from mice treated with 5-FU (n = 3), pI:pC (n = 4) or PBS (n = 4). HSCs from untreated *Mycn*$^{+/+}$*Myc*$^{+/+}$ shown in solid grey as a reference. Mean fluorescence intensities in HSC from multiple mice are plotted in

(**c**). (**d**) pI:pC treated wild-type ($n = 7$), *Mycn*$^{F/+}$Mx1-Cre^{+} ($n = 3$),*Mycn*$^{F/F}$Mx1-Cre^{+} ($n = 3$) or *Huwe1*$^{F/Y}$Mx1-Cre^{+} ($n = 5$) mice were administered a single dose of 5-FU and the absolute number of HSCs retained in their bone marrow was measured by FACS 16d later. $^{*}P < 0.05$, $^{**}P < 0.01$, $^{***}P < 0.001$ (two-tailed *t*-test). Data are representative of two experiments (mean and s.e.m. in **c,d**).

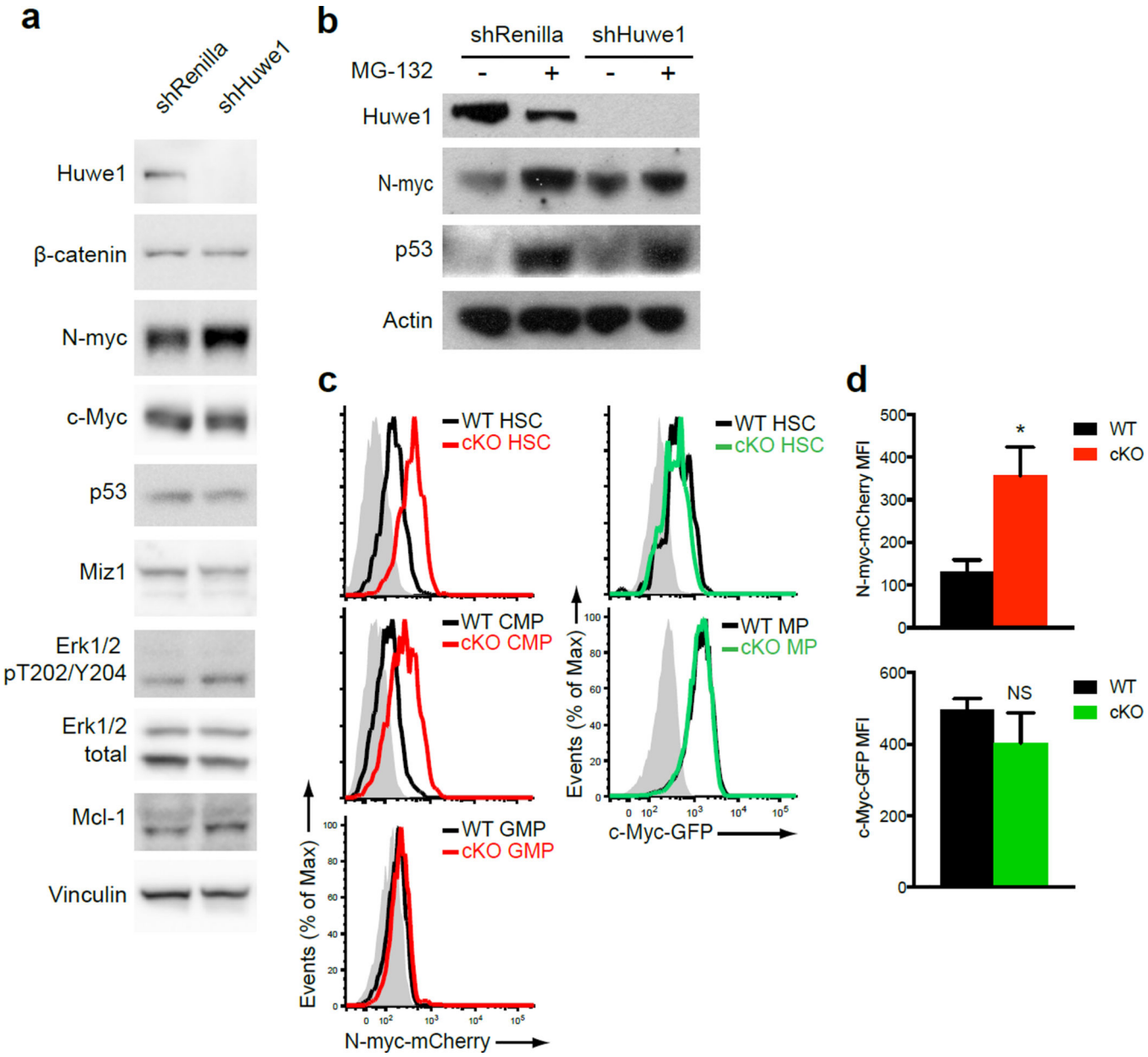

Figure 5. Loss of Huwe1 leads to accumulation of N-myc in HSCs

HPC-7 cells were infected with a retroviral shRNA construct targeting either *Huwe1* or *Renilla* luciferase as a control and selected for expression with puromycin (2 μg/ml) for 48h. (**a**) Protein extracts were probed by immunoblot with the indicated antibodies. Vinculin was used as a loading control. (**b**) Immunoblot for N-myc and p53 in HPC-7 cells expressing control or Huwe1 shRNA after for 3h of proteasome inhibition with 10mM MG-132 or DMSO. β-actin was used as a loading control, (**c**) Histograms of mCherry and GFP fluorescence measured by FACS in gated HSC, CMP, GMP and MP (total $Lin^{-}Kit^{+}Sca1^{-}$) from bone marrow of $Huwe1^{F/Y}$ Mx1-Cre^{+} $Mycn^{M/M}Myc^{G/G}$ ($n = 4$) or $Huwe1^{+/Y}$ Mx1-Cre^{+} $Mycn^{M/M}Myc^{G/G}$ ($n = 4$) mice, 2 wk after treatment with with pI:pC. Fluorescence in these populations from $Mycn^{+/+}Myc^{+/+}$ mice is shown in solid grey as a reference. Mean

fluorescence intensity from multiple mice is plotted in (**d**). Data are representative of two experiments (**a-b**) or two experiments with four biological replicates each (*$P = 0.0008$, two-tailed *t*-test, mean and s.e.m. in **c-d**).

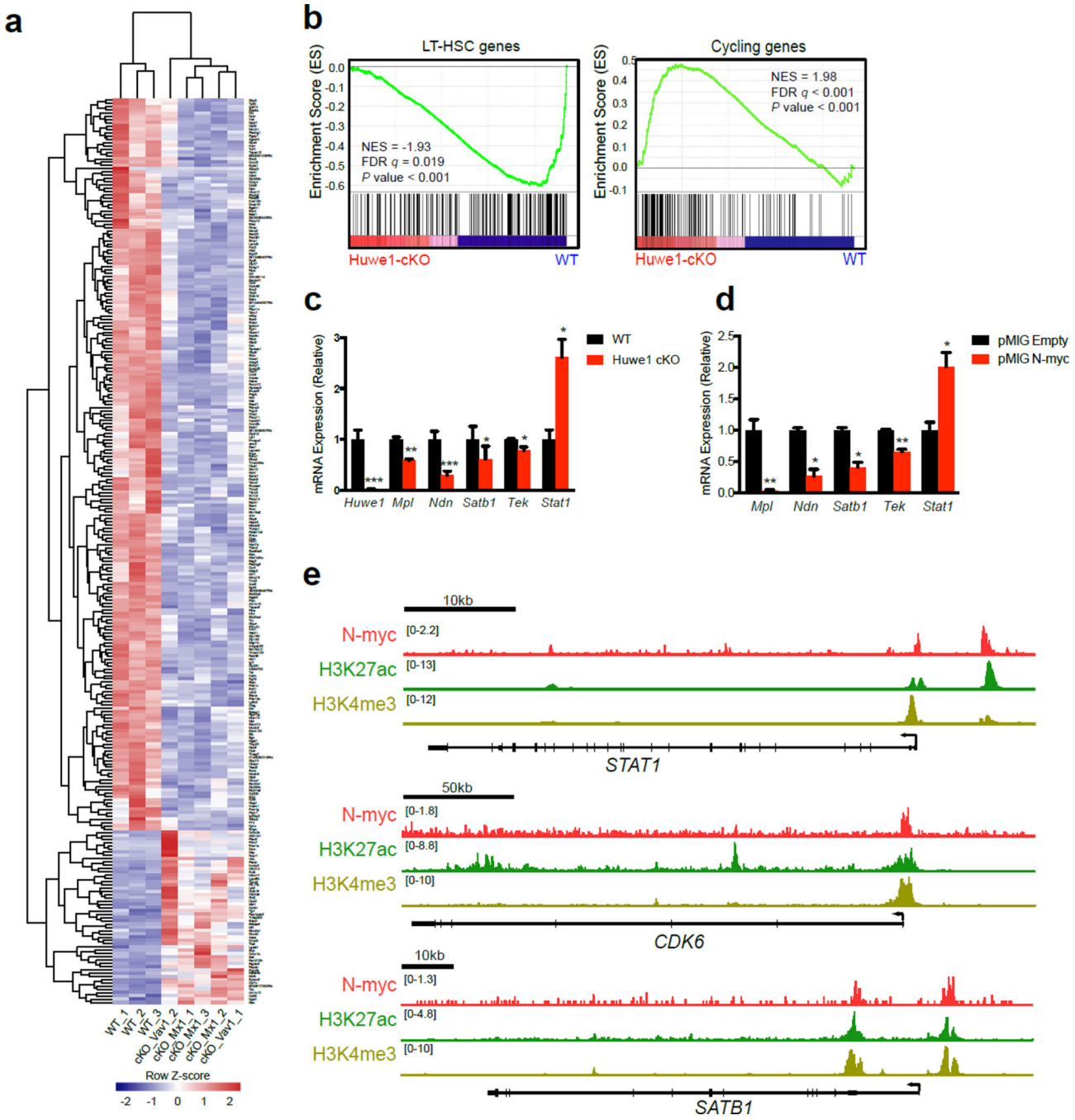

Figure 6. Stem cell gene expression programs repressed in *Huwe1*-deficient HSC

(**a**) Heat map of genes that are differentially expressed (fold change > 2, FDR $q < 0.05$) between wild type ($N = 3$) and *Huwe1*-deficient HSC (Mx1-cKO: $N = 3$; Vav1-cKO: $N = 2$) sorted from individual mice as determined by high-throughput RNA sequencing. (**b**) Gene set enrichment analysis (GSEA) was performed by searching the Molecular Signatures Database (C2: curated v4.0) for gene sets that were significantly enriched among either the wild-type or *Huwe1*-deficient HSCs. Enrichment plots for two of the most highly significant gene sets are shown. (**c**) Expression changes in Huwe1 cKO HSCs for selected genes were

validated by qRT-PCR. (**d**) HSCs were sorted from the bone marrow of wild-type mice and infected with a retrovirus to ectopically express N-myc or an empty vector control. After 48h of *in vitro* culture, transduced HSC were sorted on the basis of GFP expression and RNA was isolated to quantify changes in gene expression by qRT-PCR. Expression values in (**c-d**) determined by the $\Delta\Delta C_T$ method using *Gapdh* as an internal control. (**e**) ChIP-seq tracks showing enrichment of N-myc, histone H3K27ac and H3K4me3 at selected human gene loci. $*P < 0.05$, $**P < 0.01$, $***P < 0.001$ (two-tailed *t*-test). Data are representative of three biological replicates (**c-d**; mean and s.e.m.) or four technical replicates (**e**).

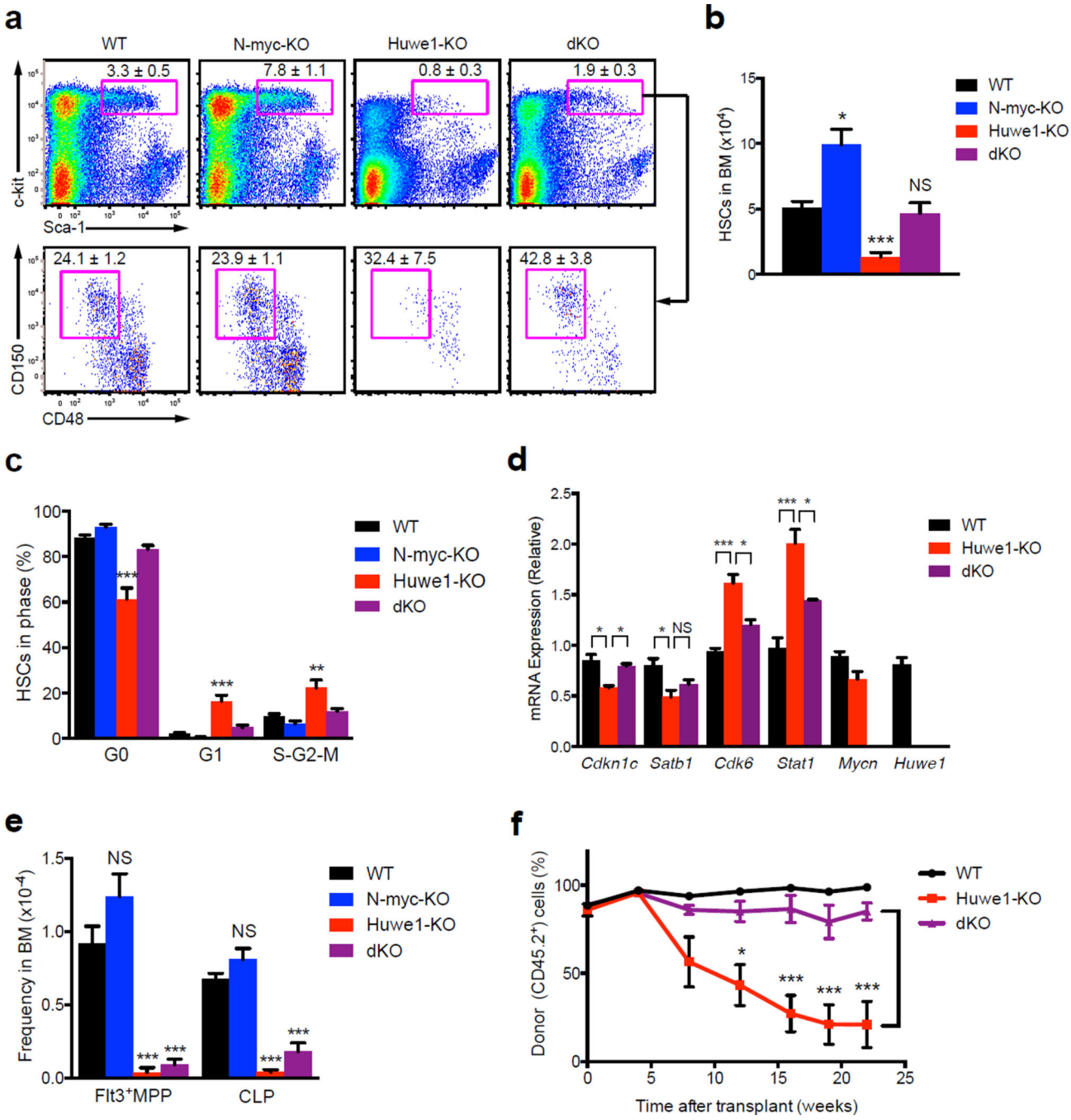

Figure 7. Depletion of *Mycn* rescues HSC function in *Huwe1*-deficient mice

Age-matched cohorts of *Huwe1*$^{+/Y}$*Mycn*$^{+/+}$Mx1-Cre^{+} (WT) ($n = 9$), *Huwe1*$^{+/Y}$*Mycn*$^{F/F}$Mx1-Cre^{+} (N-myc–KO) ($n = 5$), *Huwe1*$^{F/Y}$*Mycn*$^{+/+}$Mx1-Cre^{+} (Huwe1–KO) ($n = 10$) and *Huwe1*$^{F/Y}$*Mycn*$^{F/F}$Mx1-Cre^{+} (dKO) ($n = 8$) mice were treated with pI:pC and sacrificed 4 months later for analysis. (**a**) Flow cytometry of bone marrow showing average frequency ± s.e.m. of c-kit^{+} Sca1^{+} cells (HSPCs) within the Lin^{-} population (upper panels) and further sub-fractionated to identify CD48^{-}CD150^{+} cells (HSCs) (lower panels). (**b**) Absolute number of HSCs within bone marrow of mice of the indicated genotypes. (**c**)

Average frequency of bone marrow HSCs from each genotype that are in cell cycle phases as determined by intracellular Ki67/DAPI staining. (**d**) qRT-PCR analysis of mRNA expression in HSCs sorted 2 weeks after pI:pC treatment from the bone marrow of indicated genotypes. *Gapdh* was used as an internal control and values were normalized to WT. (**e**) Frequency of early lymphoid progenitors in bone marrow of mice analyzed in (**a**). (**f**) Frequency of donor-derived ($CD45.2^+$) myeloid cells ($CD11b^+$) in peripheral blood of recipient mice transplanted with 1×10^6 bone marrow cells from indicated genotypes ($n = 5$, per group). Recipients were injected with pI:pC 4 weeks after transplant. $^*P < 0.05$, $^{**}P < 0.01$, $^{***}P < 0.001$. Data are representative of two pooled experiments (**a-c,e**; mean and s.e.m.), one experiment with three biological replicates (**d**; mean and s.e.m.) or two experiments (**e**; mean and s.e.m.).